

## Coherent grazing exit x-ray scattering geometry for probing the structure of thin films

Franz Pfeiffer<sup>a)</sup>

*Swiss Light Source, Paul Scherrer Institut, CH-5232 Villigen, Switzerland*

Wei Zhang and Ian. K. Robinson

*Department of Physics, University of Illinois, Urbana, Illinois 61801*

(Received 28 July 2003; accepted 16 January 2004)

We demonstrate a diffraction geometry which provides strong sensitivity to the microstructure of thin films. While a coherent beam of x rays is being reflected from the surface of the sample, measurements were made of the scattering of the exit beam below the critical angle for total external reflection. This results in a strong signal with speckle modulations that are characteristic of the internal arrangement of grains at different depths within the film. © 2004 American Institute of Physics. [DOI: 10.1063/1.1669061]

One of the strengths of x-ray diffraction as an analytic method is that the internal structure of materials can be measured nondestructively because of the penetrating property of x rays. For a granular material, such as a polycrystalline metal, the average grain size can be deduced directly from the angular width of the scattered beam. This has led to the routine use of x-ray diffraction in metallurgical analysis.

It is known from sectional transmission electron microscopy that evaporated metallic thin films contain a hierarchy of grain sizes distributed over the depth of the film.<sup>1</sup> Because conventional x-ray scattering methods are not sensitive to the depth within the film, powerful methods have been introduced based on the refraction of the beam near the critical angle for total external reflection,  $\alpha_c$ .<sup>2</sup> When an x-ray beam impinges on a surface with its incidence angle  $\alpha_i$  below  $\alpha_c$ , it reflects totally and creates an evanescent wave inside the sample with a depth that can be varied from a few to a few hundred nanometers. This has been exploited in the method of grazing incidence small angle x-ray scattering, which is widely used for the study of nanostructures assembled on substrates.<sup>3</sup>

Reciprocity ensures that the same refraction behavior applies to a beam emerging from the sample at an angle of exit,  $\alpha_f$ , near  $\alpha_c$ . Using both  $\alpha_i$  and  $\alpha_f$  near  $\alpha_c$  is a method to obtain even stronger surface sensitivity. Here we demonstrate that use of a beam with  $\alpha_i > \alpha_c$  allows sufficient penetration to probe deep inside a thin film, yet, by analysis of the angular distribution in  $\alpha_f$ , still allows depth profiling of its internal microstructure. We show that the surface contributions can be avoided and still result in a strong enough signal that coherence effects can be exploited to further enhance the understanding.

Coherent diffraction from a granular microstructure results in a speckled modulation of what would otherwise be diffuse scattering with an overall width that is inversely related to the grain size. The size of the speckles is inversely related to the beam size, but also includes the effects of refraction of the incident or exit beams. In this experiment,

the shape of the speckles is used to diagnose the distortions of the beam that arise from the grazing exit geometry. The speckles also provide information about the specific distribution of grains under illumination, which information can be employed for detailed characterization of the sample.

Our experiments were carried out at the undulator beam-line 34-ID-C of the Advanced Photon Source using monochromatic radiation of 8.92 keV, for which the critical angle of gold is  $\alpha_c \approx 0.5^\circ$ . Coherence was achieved by use of two roller-blade slits,<sup>4</sup> placed 25 and 50 mm in front of the sample, which cut down the beam to a typical size of  $10 \mu\text{m}$  horizontally and vertically to approximately match the transverse coherence of the source. The sample investigated here consisted of a  $1000 \text{ \AA}$  thin gold film on a  $15 \times 15 \text{ mm}^2$  polished quartz substrate. The film was deposited by thermal evaporation at room temperature. Before the deposition of the gold film a chromium adhesion layer of only a few Ångstrom was evaporated under the same conditions. Typical values for the rms surface roughness  $\sigma$  of gold films deposited under these conditions are less than  $10 \text{ \AA}$ . The original surface roughness of the polished quartz substrate was  $4.5 \text{ \AA}$ .

This thin film sample was laid horizontally on the principal axis of the ultrahigh vacuum diffractometer. It was tilted forward to allow illumination at an angle of  $\alpha_i$  as illustrated in Fig. 1. A direct illumination charge-coupled device (CCD) x-ray camera with a pixel size of  $22.5 \mu\text{m}$  was placed on the detector arm of the diffractometer at 2.46 m from the sample. The measurements described here were all made in the forward-scattering direction, below the reflected beam with the CCD subtending an angular range  $0 < \alpha_f < \alpha_c$  vertically, as shown.

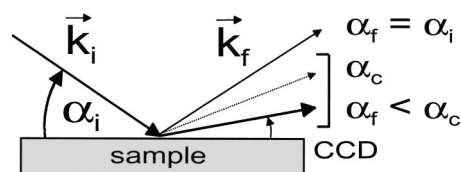


FIG. 1. Sketch (sideview) of the geometry used in the experiment. The out-of-plane directions, to which we refer by the  $x$  coordinate or  $\phi$  angle, lie perpendicular to the page and are not shown here.

<sup>a)</sup>Electronic mail: franz.pfeiffer@psi.ch

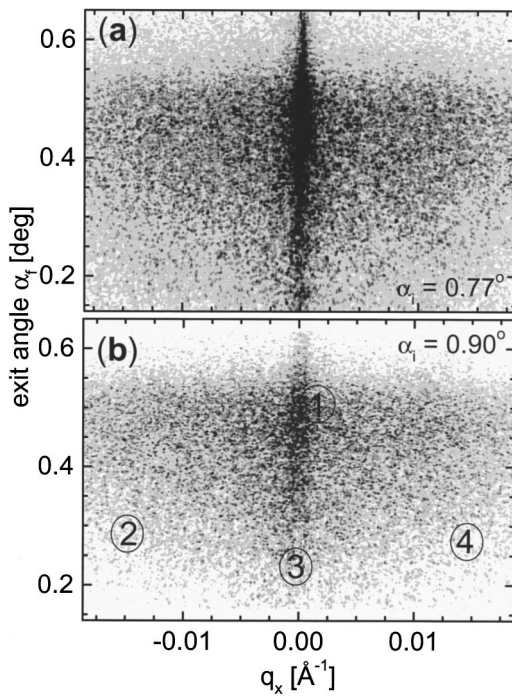


FIG. 2. Linear contour plots of the measured intensity distribution in the detector plane (CCD) as a function of the lateral momentum transfer  $q_x$  and the exit angle  $\alpha_f$  for fixed angles of incidence  $\alpha_i = 0.77^\circ$  (a) and  $\alpha_i = 0.90^\circ$  (b).

Three general components to the scattering from an inhomogeneous sample with a well-defined surface are expected under these conditions. A specular beam, with the same shape and propagation properties as the incident beam, is expected with intensity given by the Fresnel law, but reduced by any surface roughness present. A “ridge” of off-specular scattering, but lying within the scattering plane, is usually attributed to the missing specular intensity due to the roughness.<sup>5,6</sup> The extended ridge shape is due to the extreme grazing geometry. Finally, there is a generally diffuse scattering coming from the distribution of bulk grains. Both of these diffuse components acquire a speckled appearance when a coherent beam is used.<sup>7</sup> The intensity of both diffuse components becomes enhanced when  $\alpha_f \approx \alpha_c$  by the electric-field transmission function of the interface<sup>8</sup> to produce a so-called “Yoneda” peak. All three of these features are seen in the data in Fig. 2(a), with the general (doubly off-specular) diffuse scattering taking a striking “triangle” shape.

The two diffuse components are distinct in the sense that the “ridge” is tied to the surface while the “triangle” is tied to the inhomogeneities in the bulk material of the film. They can be conveniently separated by increasing  $\alpha_i$ , as shown in Fig. 2(b): the ridge moves upward along with the specular beam, while the triangle remains on the horizon, in the plane of the surface with  $0 < \alpha_f < \alpha_c$ . When  $\alpha_i$  is increased, the intensity in the “triangle” becomes weaker, but not dramatically. The total exposure time for the data of Fig. 2 was typically less than 5 min. This demonstrates that it is possible to separate the signal from the near-surface microstructure of the thin film from the surface morphological effects.

Each value of  $\alpha_f$  in the region below  $\alpha_c$  corresponds to a different evanescent wave  $\Psi(\alpha_f)$  inside the sample. Its amplitude decreases with the distance,  $z$ , from the dielectric

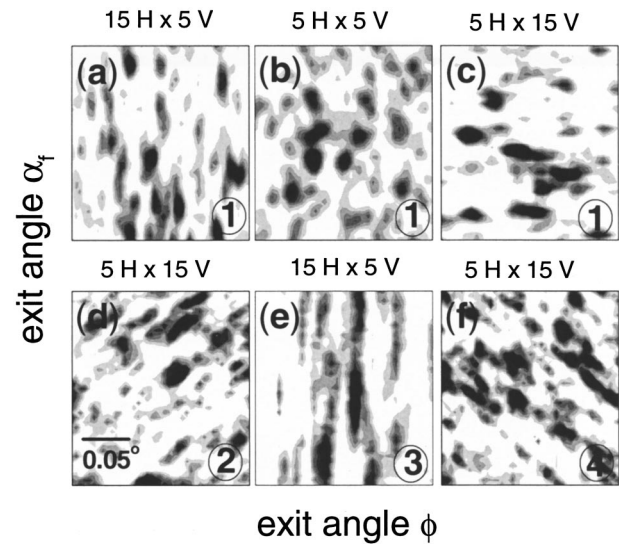


FIG. 3. Enlarged images of the measured speckle diffraction pattern at different positions [marked by encircled numbers, corresponding to Fig. 2(b)]. The entrance slit settings for each panel are given by the size of the slit gap (in  $\mu\text{m}$ ) followed by capital letters “H” or “V” to specify the horizontal (H) or vertical (V) direction, respectively.

boundary at the sample surface, according to  $\Psi(\alpha_f) = e^{-z/\Lambda(\alpha_f)}$ , where the penetration depth  $\Lambda(\alpha_f)$  is given by  $\Lambda(\alpha_f) = \lambda/2\pi(\alpha_c^2 - \alpha_f^2)^{1/2}$ .<sup>9–11</sup> The scattered signal along a horizontal slice across the triangle is therefore the square of the Fourier transform of the density function  $\rho(z)$  weighted by this decaying amplitude function. The set of profiles at different values of  $\alpha_f$  representing parallel slices across the “triangle” can be considered to be the Fourier–Laplace transform of the density distribution in the depth direction.<sup>9</sup>

$$\mathcal{I}(\alpha_f, q_x) \propto \left| \int_{-\infty}^{\infty} \int_0^{\infty} \rho(x, z) e^{-z/\Lambda(\alpha_f) + iq_x x} dz dx \right|^2. \quad (1)$$

The triangular shape results from the deeper penetration of the exit beam when  $\alpha_f \approx \alpha_c$ , which allows it to probe the finer grains at the growth interface that produces a broader distribution of the scattering. Provided the average grain size is given by  $2\pi/\Delta q_x$ , where  $\Delta q_x$  is the width of the scattering distribution along a horizontal slice through the triangle, we estimate grain sizes ranging from 30 nm (for  $\alpha_f \approx \alpha_c: \Delta q_x \approx 0.021 \text{\AA}^{-1}$ ) to 210 nm (for  $\alpha_f \approx \alpha_c/2: \Delta q_x \approx 0.003 \text{\AA}^{-1}$ ).

The shape of the speckles, which arise because of the coherent illumination of the sample, is seen to vary with  $\alpha_f$ : the speckles are rounder near  $\alpha_f \approx \alpha_c$  and become elongated in the vertical direction near  $\alpha_f = 0$  (surface plane). This is due to a simple geometric effect, for which the apparent shape of the beam on the sample as seen by the detector needs to be considered. The footprint of the beam on the sample is strongly elongated at grazing incidence by a factor of  $1/\sin \alpha_i$ . When  $\alpha_f \approx \alpha_i$ , the view from the detector is foreshortened by the same amount, producing symmetric (round) speckles. However, whenever  $\alpha_f < \alpha_i$ , the  $1/\sin \alpha_f$  foreshortening seen by the detector is stronger, so that the speckles become elongated in the vertical direction. This is what is observed in the enlargements of the diffraction pattern in Fig. 3.

The shape of the speckles also changes with the dimensions of the beam, which is demonstrated in Fig. 3. When the entrance slits are made narrower in the vertical, the speckles become elongated in the horizontal and *vice versa*. It is interesting to note that the speckle elongation of the sides of the doubly off-specular “triangle” feature can be diagonal in the case of a  $5\ \mu\text{m}$  ( $H$ )  $\times$   $15\ \mu\text{m}$  ( $V$ ) incident beam. This is explained by the foreshortening argument above: whenever the in-plane scattering angle  $\phi$  is about the same size as  $\alpha_f$ , the beam footprint appears from the detector to be inclined at  $\approx 45^\circ$ .

Rotation of the sample about a vertical axis,  $\omega$ , perpendicular to the beam led to interesting evolution in the distribution of the speckles. Even though the scattering angle was a small fraction of a degree,  $0.01^\circ$  steps of  $\omega$  were sufficient to shift the speckles by their width. The speckles on the left side of the “triangle” pattern were seen to move upwards, while those on the right side moved down, while maintaining their local arrangement. The speckles in the off-specular “ridge” did not change. This swirling motion of the speckles is consistent with the three-dimensional arrangement of speckles expected from an array of small grains confined to a thin sheet, as discussed previously.<sup>12</sup> In reciprocal space, the speckles are considerably extended in the out-of-plane direction, but they become rounded by their intersection with the Ewald sphere construction of what is seen by the detector. When the sample angle  $\omega$  is rotated, the point of intersection slides up or down, depending on which side of the “triangle” pattern is considered, as found.

The new geometry described in this letter will find widespread applicability to the study of the microstructure present in polycrystalline films. The primary contrast mechanism is the lower density associated with the domain walls, rather than the domains of the material itself. It is therefore highly sensitive to smaller domains. The diffraction data are over-sampled with respect to the spatial Nyquist frequency, so in principle it should be invertible into three-dimensional im-

ages of the interior structure of the illuminated volume of the film.<sup>13</sup> It is envisaged that the technique will find important applications in the study of the coalescence and maturation of thin films during growth, which is not readily accessible by any other technique.

The authors thank C. Benson for his help with the 34-ID-C beamline and I. Vartanyants for a series of fruitful discussions. This work was supported by the NSF under Grant No. DMR 03-08660. The 34-ID-C Coherent X-ray Diffraction facility was built with funds from NSF DMR 97-24294. The UNICAT facility is supported by the University of Illinois Materials Research Laboratory, funded by U.S. Department of Energy (DOE) under DEFG02-91ER45439, Oak Ridge National Laboratory, the National Institute of Standards and Technologies, and UOP Research & Development. The APS is itself supported by the DOE under Contract No. W-31-109-ENG-38.

<sup>1</sup>C. V. Thompson, *Annu. Rev. Mater. Sci.* **30**, 159 (2000).

<sup>2</sup>R. W. James, *The Optical Principles of the Diffraction of X-rays* (Bell, London, 1948).

<sup>3</sup>G. Renaud *et al.*, *Science* **300**, 1416 (2003).

<sup>4</sup>J. L. Libbert, J. A. Pitney, and I. K. Robinson, *J. Synchrotron Radiat.* **4**, 125 (1997).

<sup>5</sup>S. K. Sinha, E. B. Sirota, S. Garoff, and H. B. Stanley, *Phys. Rev. B* **38**, 2297 (1988).

<sup>6</sup>M. Rauscher, T. Salditt, and H. Spohn, *Phys. Rev. B* **52**, 16855 (1995).

<sup>7</sup>I. K. Robinson, J. A. Pitney, J. L. Libbert, and I. A. Vartanyants, *Physica B* **248**, 387 (1998).

<sup>8</sup>M. Born and E. Wolf, *Principals of Optics* (Pergamon, Oxford, 1980).

<sup>9</sup>H. Dosch, *Springer Tracts Mod. Phys.* **126**, 21 (1993).

<sup>10</sup>Note that the penetration depth  $\Lambda$  is mainly determined by  $\alpha_f$ , since  $\alpha_f < \alpha_i$  in our case.

<sup>11</sup>Detailed simulations have shown that the effects of the substrate–thin film interface can be neglected.

<sup>12</sup>I. K. Robinson, R. Pindak, R. M. Fleming, S. B. Dierker, K. Ploog, G. Grübel, D. L. Abernathy, and J. Als-Nielsen, *Phys. Rev. B* **52**, 9917 (1995).

<sup>13</sup>G. J. Williams, M. A. Pfeifer, I. A. Vartanyants, and I. K. Robinson, *Phys. Rev. Lett.* **90**, 175501-1 (2003).